JISSE
ISSN: 2636-4425

Journal of International Society for Science and Engineering
Vol. 3, No. 1, 01-08 (2021)

JISSE
E-ISSN:2682-3438

# A Finite Element Analysis Verification of a Machine-Trained Mathematical Model of T-Tube Hydroforming

Moataz El-Shazly[1, *], Mostafa Shazly[2], Tarek Osman [3]

[1]*Mechanical Design and Production Department, Faculty of Engineering, Cairo University, Giza 12613, Egypt*

[2]*Mechanical Engineering Department, Faculty of Engineering, The British University in Egypt, Al-Shorouk City, Cairo 11873, Egypt*

[3]*Mechanical Design and Production Department, Faculty of Engineering, Cairo University, Giza 12613, Egypt*

ARTICLE INFO

*Article history:*
*Received:2020-11-15*
*Accepted:2020-11-29*
*Online:2020-11-29*

Keywords:
Tube hydroforming
Machine learning
Multiple ridge regression
Wrinkling
Finite element modelling

ABSTRACT

*An adaptive, heuristic, nonlinear mathematical model (AHNM) was proposed to optimize the loading path of successful tube hydroforming process through adaptive minimization of the internal pressure and axial load by using Multiple Ridge Regression (Machine learning technique). The AHNM model was implemented, solved, and optimized, and it was found that increasing the number of steps and starting with small increment enables the mathematical model to capture the non-linearity of the real model, which leads to minimizing the system requirements. In this paper Finite Element Modelling (FEM) was developed to verify and test the validity and reality of the implemented loading oaths from the AHNM model for hydroforming of T-shape tube having an elliptical protrusion. The objective function was measured, and the results of minimum thickness, and maximum protrusion height were verified. Besides, the tube was formed with a well wall thickness distribution. Consequently, it is confirmed that developing an adaptive heuristic nonlinear mathematical modelling is effective for obtaining a Loading Path for Hydroforming of a Tube Having an Elliptical Protrusion.*

## 1. Introduction

The first invention to manufacture seamless copper fittings with T-protrusions using a combination of internal pressure and axial load Tube Hydroforming (THF) was by Gray, Devereaux, and Parker [1]. Due to the advances in high-pressure hydraulic systems and improvement in machine fixtures/tools, new shapes, materials, and operation principles were introduced where simultaneous control of the internal pressure and axial load is performed to produce defect-free parts, either defect by wrinkling due to excessive axial loads or bursting due to excessive internal pressure.

Most of finite element modelling (FEM) studies had been performed to predict the effect of process parameters (internal pressure, axial feeding, friction coefficient, material properties, die geometry, etc.) to produce a defect-free product [2-9].

The adaptive process simulation was used to develop the hydroforming modelling process. These processes use an incremental procedure to detect the onset of defects, where at the end of each increment, load values are modified for the subsequent increments. Process parameters are adjusted to avoid the onset of wrinkling and bursting using several control techniques such as fuzzy logic had been implemented with the several algorithms [10-14], Genetic algorithm (GA) by Abedrabboaet al. [15], and iterative optimization using response surface methodology by Jansson, Nilsson, and Simonsson [16].

The objective of this work is to verify the proposed AHNM model by using finite element modelling. Objective function is measured, and the results of minimum thickness, and maximum protrusion height are verified. The AHNM model tackled the expensive complex systems by predicting the optimum loading path by proposing an approach to combine finite element

*Moataz El-Shazly, Mechanical Design and Production Department, Faculty of Engineering, Cairo University, Giza, +201271915198,

simulations and Machine Learning Techniques to express the relations between the process parameters and take into consideration the problem objective function to minimize the pressure and the applied axial load.

## 2. Adaptive Heuristic Framework

The hydroforming process was modelled in the adaptive heuristic nonlinear mathematical model (AHNM) by using machine learning algorithms (MLA). Figure 1 solves the need for real-time data or depends on historical data by using machine learning algorithms to map the relations between inputs and outputs of the FEA process. Doing that, an MLA trained on an FEA dataset would be able to predict the behavior of the material under hydroforming, thus removing the need for historic or real-time data. When the machine learning algorithms could be explicitly formulated (our case study), the preferred route is the Adaptive heuristic nonlinear mathematical (AHNM) model, where the equations obtained from the ML could be integrated into a closed-form, mathematical model.

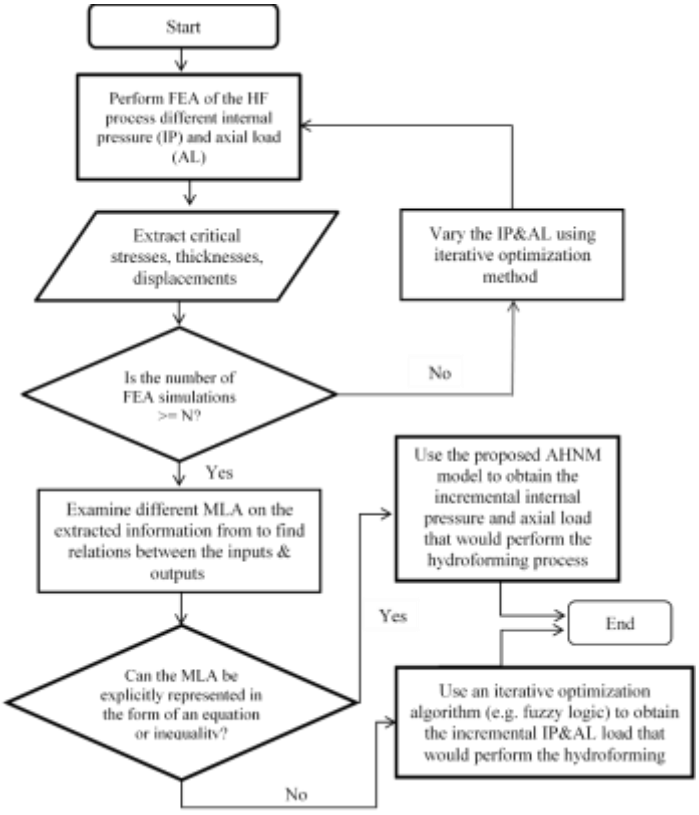


Fig. 1: The Adaptive Heuristic Framework Proposed

The FEA was performed using Simulia® 2020. A seamless copper tube (Cu=99.90%) was used. Density 8940 Kg/m3, Tensile strength (Su) & Yield strength (Sy) 310.0 MPa & 276.0 MPa, Modulus of elasticity (E) 117 GPa, Poisson ratio 0.33, Strength Coefficient (K) 315.0 MPa, Strain hardening exponent (n) 0.54. Figure 2 shows the product dimensions. Based on the iterative process proposed in Figure 3, the values of the internal pressure and axial load are obtained to produce a wrinkle-free product.

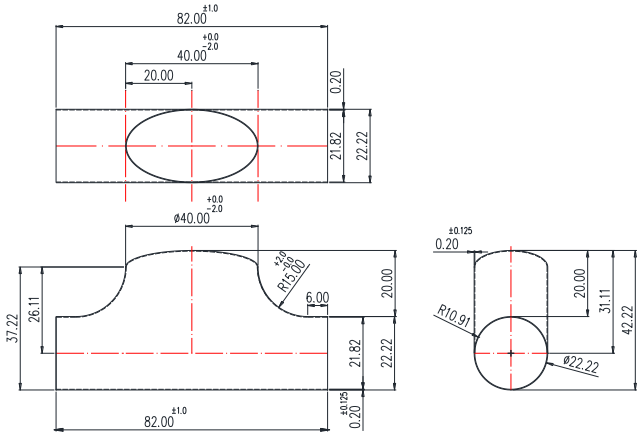


Fig. 2: Dimensions of the final product

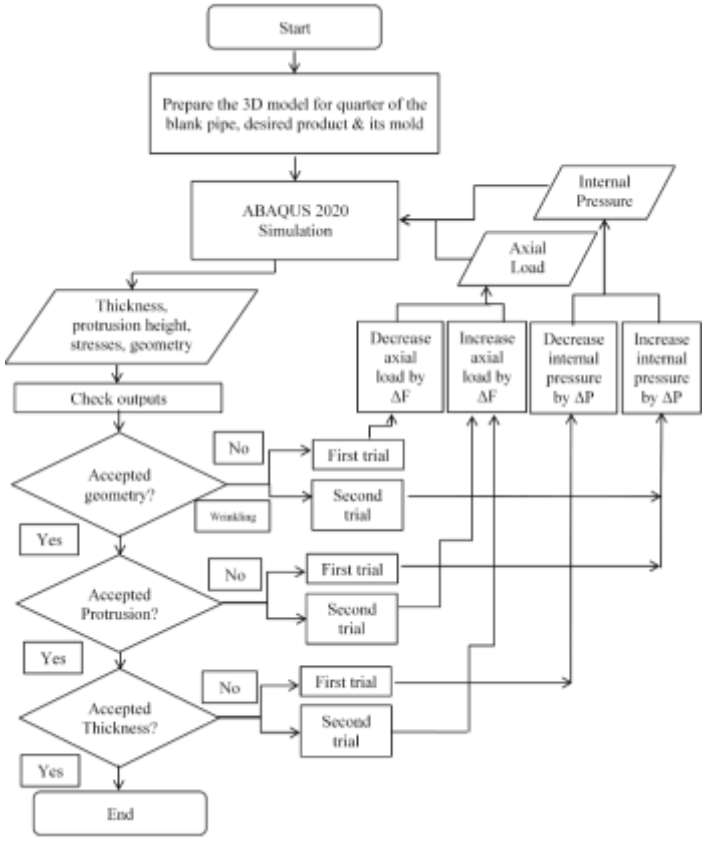


Fig. 3: Flow Chart of the Iterative Process Proposed to Produce the Initial FEM

### *2.1. Machine learning algorithms*

This paper focuses on verifying the model investigated by supervised machine learning (ML) (the input and the outputs of the process were known and labelled). ML was not by itself an optimization tool. Normally, the machine learning algorithms could only deal with several inputs and one output. It was

proposed to use a multi-input, multi-output approach. In particular, each algorithm will relate all the inputs to one output at a time (i.e. all inputs were mapped to internal pressures, then all the inputs are mapped again to the axial forces). Therefore, two distinctive equations are obtained as shown below. The inputs used here were: $MinT_t$, $MaxT_t$: minimum and maximum thickness *(mm)* at the area of the non-circular protrusion at time *t*, $MD_t$: maximum vertical displacement *(mm)* within the area of the non-circular protrusion at time *t*, $KE_t$: average kinetic energy *(mJ)* of the whole deformed part at time *t*, $IE_t$: average internal energy *(mJ)* of the whole deformed part at time *t*, $HS_t$: maximum hoop stress *(MPa)* within the area of the non-circular protrusion at time *t*, $AS_t$: maximum axial stress *(MPa)* within the area of the non-circular protrusion at time *t*, $MS_t$: maximum principal strain within the area of the non-circular protrusion at time *t*, The outputs were: $IP_t$: internal pressure *(MPa)* at time *t*, $AL_t$: axial load *(N/mm)*at time t.

The Ridge Regression, which was representable in equations, and the coefficients obtained could give insights into how the outputs are affected by the inputs and vice versa. Applying the Multiple Ridge Regression, the equations relating inputs and outputs are:

$$IP_t = 1.794648 + 0.099449\,MinT_t + 0.06269\,MaxT_t - 0.04937\,MD_t - 0.00056779\,KE_t + 0.00030773\,IE_t + 0.00381359AS_t + 0.00225969\,HS_t + 0.18261735\,MS_t \quad (1)$$

$$AL_t = 24.12692 + 8.260599\,MinT_t + 2.18032\,MaxT_t + 0.707943356\,MD_t - 2.85718919\,x10^{-3}KE_t + 4.85440054x10^{-4}IE_t - 6.90207861x10^{-2}AS_t + 7.48092522x10^{-2}HS_t - 4.57685\,MS_t \quad (2)$$

*2.2. Adaptive heuristic nonlinear mathematical (AHNM) model*

The objective of the proposed model was to obtain the optimum loading path, internal pressure, and axial load, where the non-circular protrusion and the whole tube will follow to obtain the final shape. A Multi Linear Regression learned the causal relations between the different parameters to be able to formulate mathematical forms that explained these relations, and then optimized these mathematical forms, taking into consideration the wrinkling and thinning indicators. From literature a closed-form wrinkling criteria based on instability of thin-walled tubes, Mellor [17] and Jain [18] was used to formulate the AHNM model as given in Eq. (3):

$$\varepsilon_{critical} = \frac{2}{3}n\sqrt{\left(\frac{\sigma_{axial}}{\sigma_{hoop}}\right)^2 - \frac{\sigma_{axial}}{\sigma_{hoop}} + 1} \quad (3)$$

where $\varepsilon_{critical}$ is the strain at which instability occurs, n isthe hardening exponent, $\sigma_{axial}$ is the axial stress within the tube, and $\sigma_{hoop}$ is the circumferential stress within the tube. It was assumed that the axial and the hoop stresses are approximately equal to the maximum and the second maximum principal stresses obtained from the FEA simulations. Eq. (3) will be incorporated into the model proposed below. Necking indicator used accounts for the minimum thickness of the model, and must not be less than a minimum allowable thickness constraint (MIAT). The nonlinear mathematical model variables are: Objective function Minimize

$$\sum_{t=1}^{N}(IP_t + AL_t) \quad (4)$$

where *t* is the period (1 to N) and N is the total number of periods

Constraints are equations 1, 2 above and:

$$MS_t \le \frac{2}{3}n\sqrt{\left(\frac{AS_t}{HS_t}\right)^2 - \frac{AS_t}{HS_t} + 1} \quad (5)$$

$AS_t = HS_t + C$, where C is a constant (6)

$MD_{t+1} = MD_t + S$, where S is a constant of maximum allowable vertical displacement per period (7)

$KE_t \le IE_t$*Y, where Y is a constant between 5-10% (8)

MIAS$\le AS_t, HS_t \le MAS$, where MIAS is the minimum allowable deformation stress, and the MAS is the maximum allowable deformation stress (9)

$MIAT \le MinT_t \le MAT$, where MIAT is minimum allowable thickness and MAT is the maximum allowable thickness (10)

$MD_N = FH$, where N is the last period, and FH is the final height of the non-circular protrusion (11)

$MinT_t, MaxT_t, MD_t, KE_t, IE_t, AS_t, HS_t, MS_t \in R^+$, where $R^+$ is the set of positive real (12)

The objective function (4) is to minimize the total internal pressures and axial loads during the process. Constraints (1) and (2), using the ridge regression, represent the relations between the outcomes of the several FEAs of the hydroforming process of the non-circular protrusion. Constraint (5) ensures that the maximum strain in the deformed part including the non-circular protrusion does not exceed the strain that could cause plastic instability.

## 3. Results and discussion of proposed AHNM model

The AHNM model was implemented using Pyomo, an open-source optimization formulation models written in Python language with a diverse set of optimization capabilities. Since Pyomo was not a solver but a mathematical algebraic modelling language, a solver named IPOPT (Interior Point OPTimizer) was used to solve the nonlinear AHNM model. To solve the model, the following parameters were used:

*N = 10 periods, C = 5 MPa, S = 2 mm, Y = 5%, MIAS = 300 MPa, MAS = 340 MPa, MIAT = 0.15 mm, MAT = 0.3 mm*

*3.1. Results and discussion of proposed AHNM model*

The output value of the objective function was 42.5, which represents the average of the total algebraic summation of internal pressures and axial loads that were used through the total hydroforming period. The model obtained a minimum thickness of 0.15 mm in the non-circular protrusion part. The optimized maximum axial stress in the deformed part was 300 MPa, and the optimized maximum hoop stress was 295 MPa. The maximum

principal strain to avoid plastic instability (wrinkling and necking) was 0.363. It should be noted that the maximum allowed vertical displacement per period is 2 mm. The optimum results for the internal and axial load obtained are shown in Figure 4.

The obtained paths of internal pressure and axial load show that the optimum path was always linear with equal steps of protrusion height. The effect of the loading steps on the system requirements (summation of internal pressure and axial load at certain protrusion height) and the maximum protrusion height can be reached for the tee joint was also investigated. There were 10 equal steps, where each step would increase the height of the protrusion by 2 mm. Table 1 shows different arrays of steps which were solved using the AHNM model to produce new forming paths.

Each array steps express the input in the AHNM model, where the output is an internal pressure value and axial load value at each step (loading path). Comparing these values indicates that the step numbers and values of each array are directly affecting the solver objective function. The minimum values for the objective function are for Arrays No. 5 and No. 7 with values of 40.7 and 39.71, respectively.

The differences between the results of the internal pressure and axial load of each array cause the difference in the objective function, while the boundaries (first and last) values are almost the same. This shows the consideration of physical process parameter by the AHNM model. Noteworthy that the internal pressure and axial load versus the protrusion height for all arrays are straight lines with identical slope.

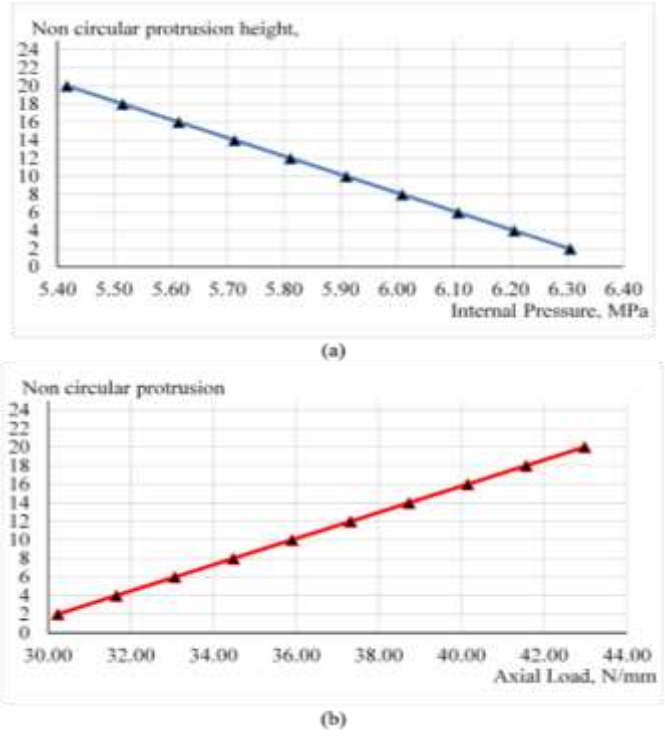


Fig. 4: Optimized AHNM Progress of (a) Internal Pressure and (b) Axial Load Through Non-Circular Tube Hydroforming

Table 1: The Arrays of Various Steps On the Vertical Displacement

| Array No. | No.1 | No.2 | No.3 | No.4 | No.5 | No.6 | No.7 |
|---|---|---|---|---|---|---|---|
| No. of steps | 10 | 10 | 10 | 10 | 10 | 50 | 50 |
| Steps values | 2,2 ,2,2 ,2,2 ,2,2 ,2,2 | 2,2 ,1,1 ,5,2 ,3,2 ,1,1 | 2,3 ,2,1 ,2,1 ,5,1 ,2,1 | 1,3 ,2,1 ,1,1 ,5,2 ,1,3 | 0.004, 0.508, 1.267, 1.719, 2.106, 2.468, 2.848, 3.254, 3.678, 2.148 | 0.001, 0.408143 *(49) | 0.001 ,0.0173 (0.001 +0.1628) ,0.0336 (0.0173 +0.1628) ……etc. |
| O.F Value | $\sum_{t=1}^{N}(IP_t + AL_t)/(\text{No. of steps})$ | | | | | | |
| | 42.5 | 42.7 | 42.8 | 41.9 | 40.7 | 41.8 | 39.71 |

### *3.2. Verification of the proposed AHNM model*

Finite element simulations (FEM) are used to analyze and verify the effect of these loading paths on the maximum protrusion height and the minimum thickness that can be reached. The AHNM model input is the protrusion height (displacement) and the outputs are the pressure and axial force, therefore it is considered as a displacement-controlled method. However, the FEM is a force-controlled method, where the pressures and forces are the inputs, and the protrusion heights (displacements) are the outputs. The output loading paths from AHNM model are applied to the FEM as amplitude values for both the internal pressure and the axial force. The amplitude time is divided into several steps equal to the array steps, and the percentage of each time value is equal to the percentage of the protrusion height at this step to the total height of the AHMN model (20 mm). At each step, the protrusion height of the AHNM model is compared with the protrusion height of the FEM at the same certain internal pressure and axial load. Besides, the internal pressure, axial load, and the minimum thickness at a protrusion height 20 mm is compared also. Tables 2 and 3 show the results of the applied loading paths from the AHNM model on FEM for the arrays. Figure 5 shows the linear relation between the loading path of AHNM model and the protrusion height for all the arrays. From the FEM results, it is clear that Arrays No.1 to No.3 which have similar starting steps with a coarse increment of 2mm, and closest values for the objective function of 42.5, 42.7, and 42.8, respectively, are almost identical curves with the same minimum thickness of 0.17mm and same system requirement of 46.64 at a protrusion height 20mm. They also reach a similar maximum protrusion of 25.17mm. However, Figures 6 (a) to (f) show the existence of wrinkling in the deformed protrusion of these arrays. Array No.4 starts with a finer increment of step (1mm) than arrays No.1 to No.3 and has better objective function value 41.9. Figures 6 (g) and (h) show a little wrinkling in the deformed protrusion of this array than previous arrays. Array No.4 tends to increase the internal pressure and decrease the axial load at the beginning of the protrusion, that gives a minimum thickness of 0.16 mm, 46.02 system requirement at a protrusion height 20 mm and the maximum protrusion that can be reached in this case is 26.95mm.

Array No. 5 is generated with 10 steps and has an identical loading path to Arrays No. 6 and 7 which are generated from 50 steps and with the same minimum thickness of 0.16mm and same system requirement of 45.20 at a protrusion height of 20 mm. In addition, approximately the same maximum protrusion of 29.61mm can be reached. This causes different values the objective function and shows a more successful model when comparing Figures 6 (i), (j) with Figures 6 (m), (n).

Arrays No. 6 and 7 don't show significant changes or improvements in the comparison as they give same minimum thickness, system requirement at a protrusion height of 20 mm, and similar maximum protrusion. However, the fine increment of steps in Array No.7 gives a better value for the objective function, 39.71, than Array No.6 (41.8). As the steps increment at the beginning of the process is the finest the Figures 6 (k) to (n) show the absence of the wrinkling in the model. Although Arrays No. 4 and 6 are closest in the values of the objective function, they are not identical loading path in the FEM. This is because Array No. 6 starts with fine steps as compared to Array No.4 with different numbers of steps, 10 for Array No. 4 and 50 for Array No. 6. This leads to fine steps and increases the number of steps in AHNM model which allowed to capture the non-linearity of the system and provide a better optimum loading path.

Based on Figure 5, the intersection between the AHNM line and the FEA curves indicates that extra linear constraint (or more) may modify the linear behavior of the AHNM to a piecewise to approach the non-linearity of the Arrays 1-7 as will have discussed mentioned in the future work.

Table 3: Results Summary of Arrays No.1 to 7 for AHNM and FEM

| Array | Results | Minimum Thickness1 (mm) | Maximum system requirement2 | Maximum protrusion height (mm) |
|---|---|---|---|---|
| AHNM | | 0.15 | 48.39 | 20 |
| Array No.1 | FEM | 0.17 | 46.64 | 25.18 |
| | Diff. % | 13.30% | 3.60% | 26% |
| Array No.2 | FEM | 0.17 | 46.64 | 25.17 |
| | Diff. % | 13.30% | 3.60% | 25.90% |
| Array No.3 | FEM | 0.17 | 46.64 | 25.17 |
| | Diff. % | 13.30% | 3.60% | 25.90% |
| Array No.4 | FEM | 0.16 | 46.02 | 26.95 |
| | Diff. % | 6.60% | 4.90% | 35% |
| Array No.5 | FEM | 0.16 | 45.2 | 29.61 |
| | Diff. % | 6.60% | 6.60% | 48% |
| Array No.6 | FEM | 0.16 | 45.2 | 29.61 |
| | Diff. % | 6.60% | 6.60% | 48% |
| Array No.7 | FEM | 0.16 | 45.2 | 29.62 |
| | Diff. % | 6.60% | 6.60% | 48.10% |

1 at 20mm protrusion height
2 Maximum (IPt+ALt) at 20mm protrusion height

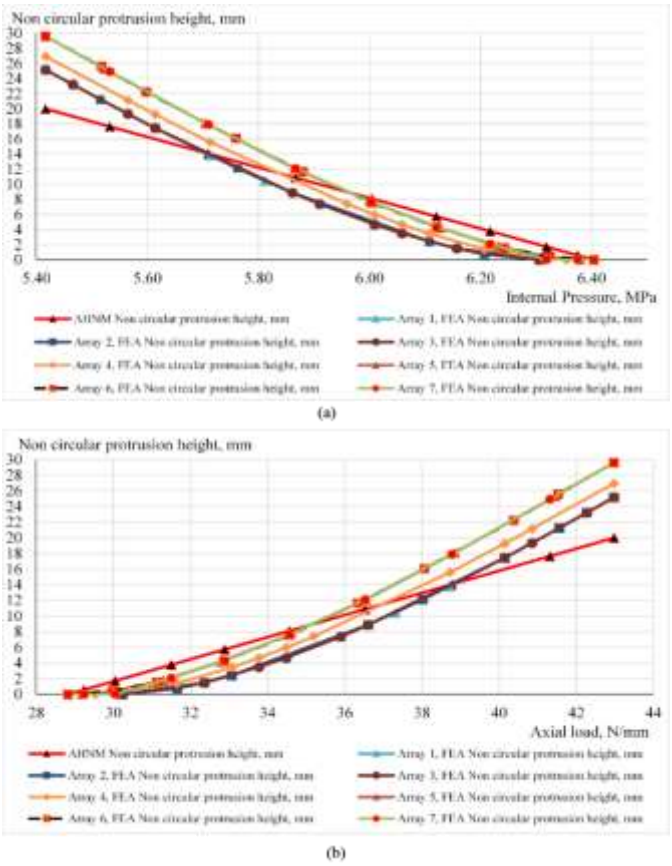


Fig. 5: Results of the AHNM and the FEM Loading Paths for Arrays No.1 to No.7 (a) Internal Pressure and (b) Axial Load

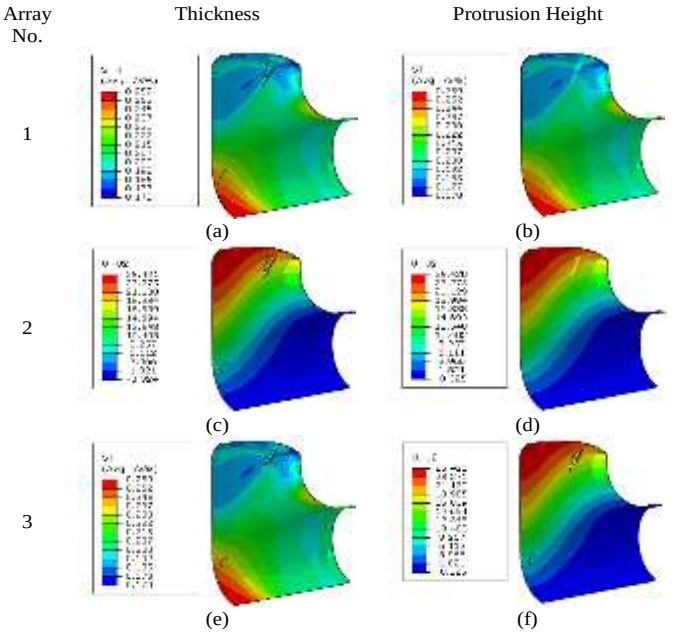


Fig. 6: (Arrays 1, 2, 3) Results of Array Thickness Distribution and Maximum Protrusion

Table 2: Arrays No.1 to No.7 Protrusion Heights for AHNM and FEM

| Protrusion height, mm | | | | | | | | | | | | | | | | | | | |
|---|---|---|---|---|---|---|---|---|---|---|---|---|---|---|---|---|---|---|---|
| Array No.1 | | | Array No.2 | | | Array No.3 | | | Array No.4 | | | Array No.5 | | | Array No.6 | | | Array No.7 | | |
| AHNM | FEM | Diff. % | AHNM | FEM | Diff. % | AHNM | FEM | Diff. % | AHNM | FEM | Diff. % | AHNM | FEM | Diff. % | AHNM | FEM | Diff. % | AHNM | FEM | Diff. % |
| 2 | 0.01 | 100% | 2 | 0.01 | 100% | 2 | 0.01 | 100% | 1 | 0.01 | 100% | 0.00 | 0.00 | 97% | 0.00 | 0.00 | 100% | 0.00 | 0.00 | 100% |
| 4 | 0.75 | 81% | 4 | 0.75 | 81% | 5 | 1.50 | 70% | 4 | 1.41 | 65% | 0.51 | 0.02 | 97% | 1.63 | 0.45 | 72% | 0.60 | 0.02 | 97% |
| 6 | 2.42 | 60% | 5 | 1.50 | 70% | 7 | 3.49 | 50% | 6 | 3.46 | 42% | 1.78 | 0.46 | 74% | 3.27 | 1.56 | 52% | 1.73 | 0.04 | 97% |
| 8 | 4.68 | 41% | 6 | 2.42 | 60% | 8 | 4.68 | 41% | 7 | 4.67 | 33% | 3.50 | 1.80 | 49% | 5.72 | 4.27 | 25% | 3.78 | 2.08 | 45% |
| 10 | 7.39 | 26% | 11 | 8.89 | 19% | 10 | 7.39 | 26% | 8 | 5.99 | 25% | 5.60 | 4.20 | 25% | 8.16 | 7.67 | 6% | 5.74 | 4.33 | 25% |
| 12 | 10.47 | 13% | 13 | 12.12 | 7% | 11 | 8.89 | 19% | 9 | 7.41 | 18% | 8.07 | 7.59 | 6% | 10.61 | 11.66 | 10% | 8.11 | 7.65 | 6% |
| 14 | 13.84 | 1% | 16 | 17.46 | 9% | 16 | 17.46 | 9% | 14 | 15.60 | 11% | 10.92 | 12.12 | 11% | 13.06 | 16.08 | 23% | 10.88 | 12.11 | 11% |
| 16 | 17.46 | 9% | 18 | 21.25 | 18% | 17 | 19.33 | 14% | 16 | 19.27 | 20% | 14.17 | 18.10 | 28% | 16.33 | 22.22 | 36% | 14.06 | 17.92 | 27% |
| 18 | 21.25 | 18% | 19 | 23.21 | 22% | 19 | 23.21 | 22% | 17 | 21.16 | 24% | 17.85 | 25.31 | 42% | 17.96 | 25.60 | 43% | 17.65 | 24.94 | 41% |
| 20 | 25.18 | 26% | 20 | 25.17 | 25.9% | 20 | 25.17 | 25.9% | 20 | 26.95 | 35% | 20.00 | 29.61 | 48% | 20.00 | 29.61 | 48% | 20.00 | 29.62 | 48.1% |

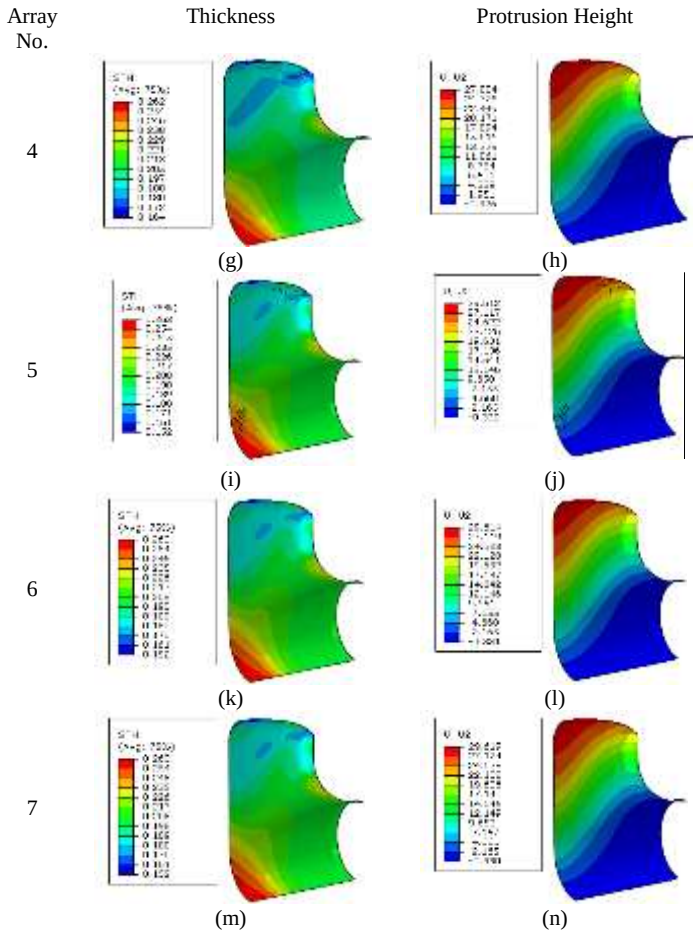


Fig. 6: (Arrays 4, 5, 6, 7) Results of Array Thickness Distribution and Maximum Protrusion

## 4. Conclusions and future work

Although the AHNM model was linear, and a percentage of difference is expected between the AHNM& FEM, the results obtained showed the ability of the ML algorithms to capture complex relations from FEA and enable their incorporation into the AHNM model to optimally predict and understand the incremental internal pressure and the axial load needed to accomplish the hydroforming process. When verifying the optimized loading path from the mathematical model by the FEM, it is found that increasing the number of steps and starting with small increment enables the mathematical model to capture the non-linearity of the real model, which leads to minimizing the system requirements.

Another improvement of the AHNM to approach the finite element software's outcome and also the real model could be achieved by improving the AHNM to include a piecewise, linear behavior that would better capture the real behavior of the hydroforming process. This can be done by the sensitive calculation of the bands into which AHNM can be split, also by including extra linear constraint (or more) this will improve the accuracy of the AHNM, while keeping the ability of the authors to incorporate a machine learning model capturing a hydroforming process in an optimization model that could be solved instantaneously.

Other parameters that could affect the tube hydroforming process (such as coefficient of friction, applying the internal pressure at different times than the axial loads can be applied – the axial load my delayed in application after applying internal pressure – and counter punch force) can be added examined and incorporated to the AHNM model.

### Conflict of Interest

The authors declare no conflict of interest.

### Acknowledgment

This research was partially supported by Misr Elgawda Company for Manufacturing & Trading, and Mechanical Design & Production department of Faculty of Engineering, Cairo University. I am thankful to my esteemed and professional colleagues in these two entities, who provided expertise that greatly assisted the research, and for their comments on an earlier version of the manuscript, that improved the manuscript significantly.

### References

[1] J. E. Gray, A. P. Devereaux, and W. M. Parker, "Apparatus for making wrought metal T's," Google Patents, 1940.

[2] K.-i. Manabe, and M. Amino, "Effects of process parameters and material properties on deformation process in tube hydroforming," Journal of materials processing technology, vol. 123, no. 2, pp. 285-291, 2002.

[3] G. Kridli, L. Bao, P. Mallick et al., "Investigation of thickness variation and corner filling in tube hydroforming," Journal of Materials Processing Technology, vol. 133, no. 3, pp. 287-296, 2003.

[4] G. Ngaile, S. Jaeger, and T. Altan, "Lubrication in tube hydroforming (THF): Part I. Lubrication mechanisms and development of model tests to evaluate lubricants and die coatings in the transition and expansion zones," Journal of Materials Processing Technology, vol. 146, no. 1, pp. 108-115, 2004.

[5] G. Ngaile, S. Jaeger, and T. Altan, "Lubrication in tube hydroforming (THF): Part II. Performance evaluation of lubricants using LDH test and pear-shaped tube expansion test," Journal of materials processing technology, vol. 146, no. 1, pp. 116-123, 2004.

[6] J. Kim, S.-W. Kim, W.-J. Song et al., "Analytical and numerical approach to prediction of forming limit in tube hydroforming," International journal of mechanical sciences, vol. 47, no. 7, pp. 1023-1037, 2005.

[7] P. Ray, and B. Mac Donald, "Experimental study and finite element analysis of simple X-and T-branch tube hydroforming processes," International Journal of Mechanical Sciences, vol. 47, no. 10, pp. 1498-1518, 2005.

[8] J. Crapps, E. Marin, M. Horstemeyer et al., "Internal state variable plasticity-damage modeling of the copper tee-shaped tube hydroforming process," Journal of Materials Processing Technology, vol. 210, no. 13, pp. 1726-1737, 2010.

[9] H. K. Yi, H. S. Yim, G. Y. Lee et al., "Experimental investigation of friction coefficient in tube hydroforming," Transactions of Nonferrous Metals Society of China, vol. 21, pp. s194-s198, 2011.

[10] A. Aydemir, J. De Vree, W. Brekelmans et al., "An adaptive simulation approach designed for tube hydroforming processes," Journal of materials processing technology, vol. 159, no. 3, pp. 303-310, 2005.

[11] S. Heo, J. Kim, and B. Kang, "Investigation on determination of loading path to enhance formability in tube hydroforming process using APDL," Journal of materials processing technology, vol. 177, no. 1-3, pp. 653-657, 2006.

[12] K.-i. Manabe, M. Suetake, H. Koyama et al., "Hydroforming process optimization of aluminum alloy tube using intelligent control technique," International Journal of Machine tools and manufacture, vol. 46, no. 11, pp. 1207-1211, 2006.

[13] [S.-h. Li, B. Yang, W.-g. Zhang et al., "Loading path prediction for tube hydroforming process using a fuzzy control strategy," Materials & Design, vol. 29, no. 6, pp. 1110-1116, 2008.

[14] [K.-i. Manabe, X. Chen, D. Kobayashi et al., "Development of in-process fuzzy control system for T-shape tube hydroforming," Procedia Engineering, vol. 81, pp. 2518-2523, 2014.

[15] N. Abedrabbo, M. Worswick, R. Mayer et al., "Optimization methods for the tube hydroforming process applied to advanced high-strength steels with experimental verification," Journal of Materials Processing Technology, vol. 209, no. 1, pp. 110-123, 2009.

[16] M. Jansson, L. Nilsson, and K. Simonsson, "On process parameter estimation for the tube hydroforming process," Journal of materials processing technology, vol. 190, no. 1-3, pp. 1-11, 2007.

[17] P. Mellor, "Tensile instability in thin-walled tubes," Journal of Mechanical Engineering Science, vol. 4, no. 3, pp. 251-256, 1962.

[18] N. Jain, "Modeling and analysis of dual hydroforming process," Texas A&M University, 2004